

See discussions, stats, and author profiles for this publication at: <https://www.researchgate.net/publication/260439784>

Imidazolyldchromanones containing non-benzylic oxime ethers: Synthesis and molecular modeling study of new azole antifungals selective against *Cryptococcus gattii*

ARTICLE in EUROPEAN JOURNAL OF MEDICINAL CHEMISTRY · APRIL 2014

Impact Factor: 3.45 · DOI: 10.1016/j.ejmech.2014.02.019

CITATIONS

4

READS

57

5 AUTHORS, INCLUDING:



Hamid Badali

Mazandaran University of Medical Sciences...

68 PUBLICATIONS 761 CITATIONS

SEE PROFILE



Hamid Irannejad

Mazandaran University of Medical Sciences

16 PUBLICATIONS 104 CITATIONS

SEE PROFILE



Preliminary communication

Imidazolychromanones containing non-benzylic oxime ethers: Synthesis and molecular modeling study of new azole antifungals selective against *Cryptococcus gattii*



Mojtaba Babazadeh-Qazijahani^a, Hamid Badali^b, Hamid Irannejad^c,
 Mohammad Hosein Afsarian^b, Saeed Emami^{c,*}

^a Student Research Committee, Faculty of Pharmacy, Mazandaran University of Medical Sciences, Sari, Iran

^b Department of Medical Mycology & Parasitology/Invasive Fungi Research Center (IFRC), Faculty of Medicine, Mazandaran University of Medical Sciences, Sari, Iran

^c Department of Medicinal Chemistry and Pharmaceutical Sciences Research Center, Faculty of Pharmacy, Mazandaran University of Medical Sciences, Sari, Iran

ARTICLE INFO

Article history:

Received 4 October 2013

Received in revised form

6 January 2014

Accepted 8 February 2014

Available online 11 February 2014

Keywords:

Antifungal activity

Azole antifungals

Cryptococcus

Chroman-4-one

Imidazole

Lanosterol 14 α -demethylase

ABSTRACT

A series of imidazolychromanone oximes containing phenoxyethyl ether moiety, as found in omoc-nazole, were synthesized and evaluated against yeasts (*Candida albicans* and *Cryptococcus gattii*) and filamentous fungi (*Aspergillus fumigatus* and *Exophiala dermatitidis*). Although the title compounds showed marginal activity against filamentous fungi but all of them exhibited potent activity against *C. gattii* (MIC values ≤ 4 μ g/mL). Among them, (3-chlorophenoxy)ethyl analog **7c** with MIC value of 0.5 μ g/mL was the most potent compound. Further molecular docking studies provided a better insight into the binding of designed compounds within the homology modeled active site of CnCYP51 (*Cryptococcus* CYP51-14 α -demethylase).

© 2014 Elsevier Masson SAS. All rights reserved.

1. Introduction

Fungal infections cause a persistent burden on human and animal health, plants and agricultural economy [1]. In human, many fungal infections are caused by opportunistic pathogenic fungi that may be endogenous flora or acquired from the environment. The incidence of fungal infections has significantly increased in recent years. The vast majority of fungal infections are due to *Candida*, *Aspergillus* and *Cryptococcus* species, especially in all categories of immunocompromised patients [2]. The immunocompromised patients including cancer patients receiving chemotherapy, organ transplant recipients and patients with AIDS are prone to fungal infections [3].

Cryptococcus neoformans is encapsulated basidiomycetous yeast that infects pulmonary organs and can disseminate widely, most

commonly to the brain and skin [4–6]. Two predominant varieties are recognized for *C. neoformans*: var. *neoformans* and var. *gattii* [7]. *C. gattii* has recently received widespread attention owing to outbreaks in British Columbia, Canada and the US Pacific Northwest, and is believed to be clinically more virulent than *C. neoformans* [8]. Infections with *C. gattii* in patients can be severe and often fatal if untreated [1].

Many drugs are available for the treatment of systemic or superficial fungal infections, but only a limited number of them are effective in the treatment of cryptococcal infections [9]. The polyene drugs such as amphotericin B and azole antifungals such as fluconazole are the most widely used drugs to treat cryptococcosis. Severe side effects such as nephrotoxicity limit the clinical usefulness of polyene drugs. Azole antifungals are generally considered as fungistatic agents and act by inhibiting lanosterol 14 α -demethylase in the ergosterol biosynthetic pathway [10]. The emergence of resistance and fungistatic rather than fungicidal activities represent limitations of current azole antifungals. Moreover, the pharmacokinetic deficiencies of azole may have a profound effect on the

* Corresponding author.

E-mail address: sd_emami@yahoo.com (S. Emami).

apparent drug resistance of azoles. For example, oral itraconazole may be less effective in the treatment of cryptococcal meningitis because of its variable oral absorption and poor cerebrospinal fluid levels [11]. Therefore, there remains an urgent need for finding new antifungal agents with proper safety and pharmacokinetics to overcome this situation and develop effective therapies especially against cryptococcal infections.

In our quest to develop newazole antifungal agents, recently we have designed 3-imidazolylchromanone oxime ethers (Fig. 1, structure A) as conformationally constrained analogs of oxiconazole [12]. Oxiconazole and most of imidazole antifungals such as miconazole, econazole, isoconazole, sulconazole and fenticonazole contain benzyl ether side chains (Fig. 1). Besidesazole antifungals with benzyl ether side chains, omoconazole is a distinctazole antifungal with non-benzylic side chain namely 2-(4-chlorophenoxy)ethyl ether. In continuation of our research program onazole antifungals, we focused our modifications mainly on the side chains of imidazolylchromanone oxime ethers, and attached 2-phenoxyethyl ether moiety to the imidazolylchromanone oxime scaffold instead of benzyl ether residue. Thus, we report here, synthesis and antifungal activity of imidazolylchromanone O-(phenoxyethyl)oxime ethers (Fig. 1, structure B).

2. Chemistry

The synthesis of target compounds imidazolylchromanone O-(phenoxyethyl)oxime ethers **7**, starting from 4-chromanone (**1**) and phenol derivatives **5** is outlined in Scheme 1. Firstly, 4-chromanone (**1**) was brominated with copper (II) bromide to give 3-bromo-4-chromanone (**2**). Compound **2** was reacted with hydroxylamine

hydrochloride in methanol to afford the corresponding oxime **3**. Reaction of 3-bromo-oxime derivative **3** with imidazole in DMF offered 3-imidazolyl-4-chromanone-(E)-oxime (**4**) [12]. On the other hand, phenol derivatives **5** were refluxed with 1-bromo-2-chloroethane in butan-2-one and converted to the corresponding phenoxyethyl chloride derivatives **6**. In the final step, (E)-oxime **4** was reacted with phenoxyethyl chloride derivatives **6** in the presence of NaH in DMF to give (E)-oxime ether derivatives **7**.

The structures of final compounds **7a–f** were fully characterized by IR, ^1H NMR, ^{13}C NMR and MS spectral data. Representatively, the spectral studies of compound **7a** are discussed here. In the IR spectrum of compound **7a**, a medium band due to the C=N of oxime moiety was appeared at 1601 cm^{-1} . In the ^1H NMR, the CH_2CH_2 unit of phenoxyethyl moiety displayed two triplet signals at 4.32 and 4.54 ppm with coupling constants of 4.4 Hz. The hydrogens located on the C-2 position of chroman ring were appeared at 4.70 and 5.01 ppm as doublets of doublets. The geminal coupling constant of the latter hydrogens was 12.0 Hz. The observed peak at 5.64 ppm was attributed to the H-3 of chroman ring. The resonances of *ortho* and *para* hydrogens of phenoxy group and H-6 and H-8 of chroman ring were occurred in the range of 6.90–7.18 ppm. The H-3 and H-5 of phenoxy group showed absorption at 7.28 ppm. A triplet at 7.46 ppm is attributed to the H-7 of chroman structure. The H-5 of chroman ring was appeared downfield at 8.57 ppm due to the deshielding of (E)-oxime functionality. The hydrogens of imidazole ring were observed at 7.68, 7.72 and 9.22 ppm. Since the compound **7a** was prepared as nitrate salt, thus the downfield shift of the latter protons is due to the protonation of imidazole ring.

In the ^{13}C NMR of compound **7a**, the aliphatic carbons of chroman core (C-2 and C-3) showed upfield signals at 74.0 and

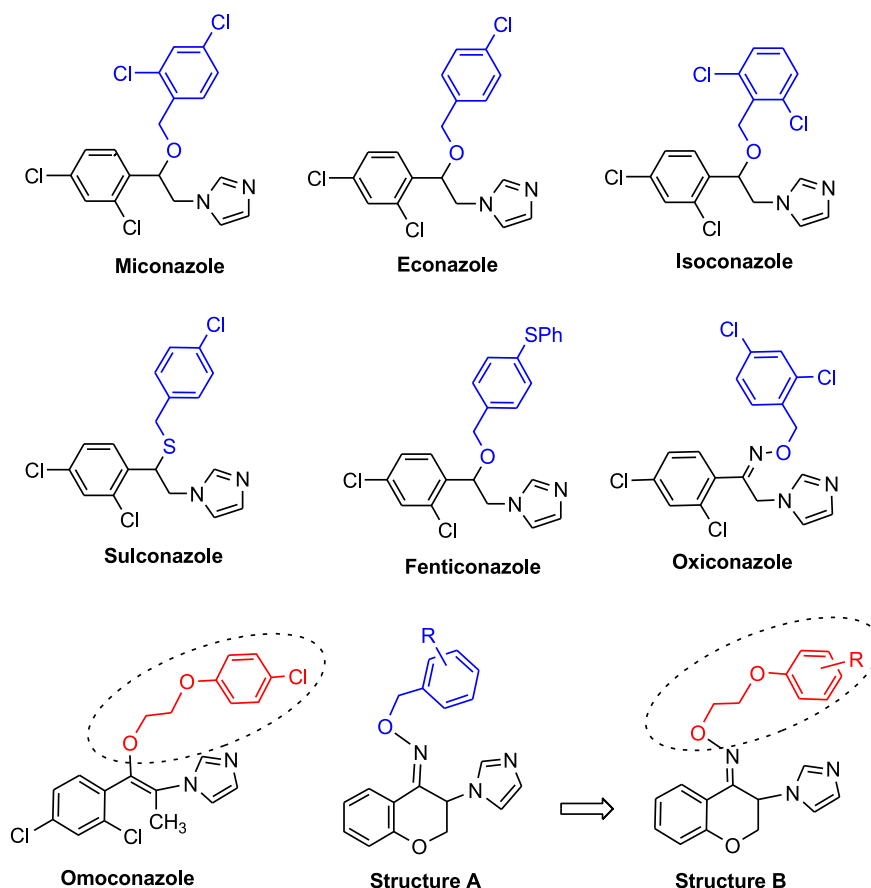
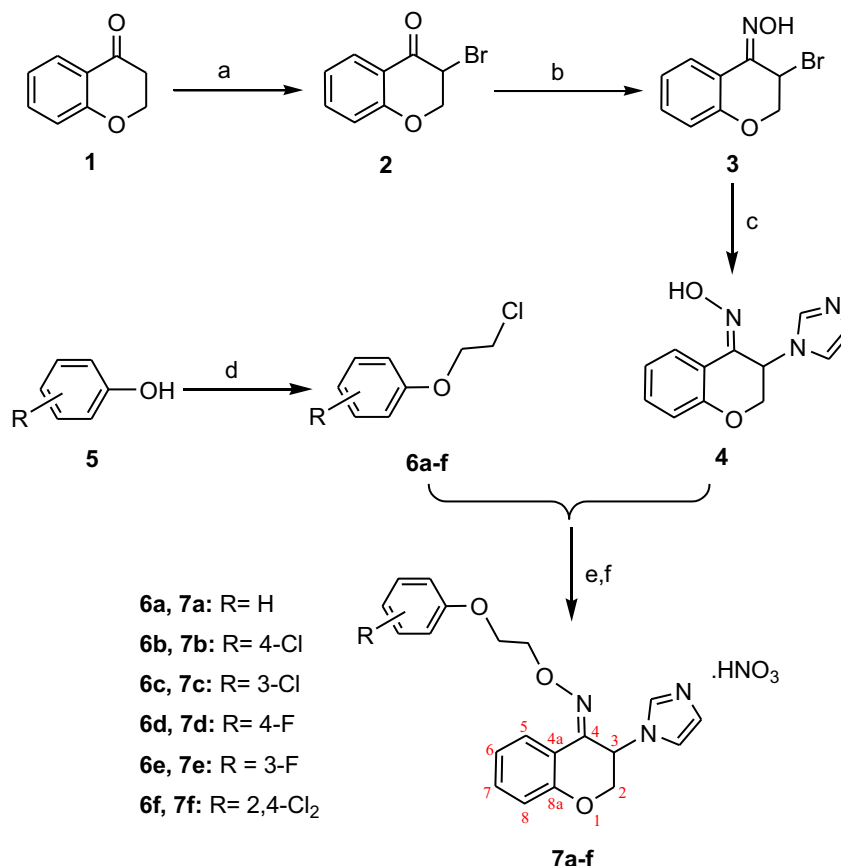


Fig. 1. Structures of representativeazole antifungals containing benzyl ether side chain, omoconazole asazole antifungal bearing 2-(4-chlorophenoxy)ethyl ether fragment, and designed 3-imidazolylchromanone oxime ethers (structure B) as non-benzylic analogs of structure A.



Scheme 1. Synthesis of imidazolylchromanone *O*-(phenoxyethyl) oxime ethers **7**. Reagents and conditions: (a) copper (II) bromide, CHCl₃-EtOAc, reflux; (b) hydroxylamine hydrochloride, MeOH, rt; (c) imidazole, DMF; (d) 1-bromo-2-chloroethane, butan-2-one, reflux; (e) NaH, DMF; (f) propan-2-ol, 65% HNO₃.

55.7 ppm, while the unsaturated C=N carbon (C-4) showed absorption at downfield region of 158.3 ppm. The signals related to the aromatic carbons of chroman ring were located at 113.5, 117.6, 120.7, 131.4, 133.2 and 141.7 ppm. The resonances of imidazole carbons C-2, C-4 and C-5 were occurred at 135.3, 121.8 and 121.0, respectively. The peaks at 65.8 and 67.1 were assigned for OCH₂-CH₂O unit. The phenoxy group showed four signals at 114.5, 120.5, 129.5, and 154.8 ppm.

The mass spectral data of compound **7a** provided further evidence of its structure. The molecular ion peak was observed at the expected *m/z* value of 349.

The (*E*)-configuration of compounds **7a–f** was readily established by ¹H NMR spectral data. Particularly, proximity of the oxime oxygen to the C-5 hydrogen of chroman ring in (*E*)-isomers result in downfield shift of the H-5 (δ H-5 > 8.5 ppm) respect to that of (*Z*)-oxime ethers (δ H-5 ≤ 7.9 ppm) [12]. The investigation of ¹H NMR spectral data revealed that the chemical shifts of C-5 proton in oxime ethers **7a–f** were in the range of 8.53–8.57 ppm. Thus, the orientation of the oxime ether moiety of compounds **7a–f** was assigned to be of (*E*)-geometry.

The compounds **7a–f** possess a chiral center at C-3 position of chroman ring. Substantially, the bromination of 4-chromanone (**1**) at C-3 position is not stereoselective. Thus, the originated intermediates **2–4** were as a mixture of enantiomers and as well the target compounds **7a–f** were obtained as a racemic mixture.

3. Biology

The antifungal activity of target compounds against yeasts (*Candida albicans* and *C. gattii*) and filamentous fungi (*Aspergillus*

fumigatus and *Exophiala dermatitidis*) were evaluated in vitro. The minimal inhibitory concentrations (MICs) of test compounds were determined by the micro-broth dilution method in 96-well microplates according to the CLSI methods for yeasts and filamentous fungi [13,14]. Briefly, compounds were dissolved in DMSO and serially diluted in growth medium. The inoculum suspension was added to each well and incubated at 35 °C. MIC was defined as the minimum inhibitory concentration of test compound which resulted in total inhibition of the fungal growth. All susceptibility testing was performed in triplicate.

4. Results and discussion

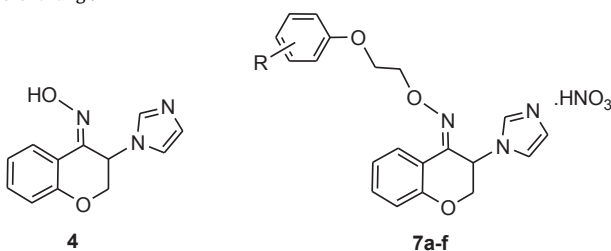
4.1. Antifungal activity

The MIC values of target compounds **7a–f** in comparison with those of parent 3-imidazolyl-4-chromanone oxime (**4**) and standard drugs fluconazole and itraconazole were summarized in Table 1. Generally, the parent oxime **4** showed no activity against all fungal species. Furthermore, all title compounds **7a–f** were inactive against *C. albicans* (MIC values >64 µg/mL). In contrast, all compounds exhibited potent activity against *C. gattii* (MIC values = 0.5–4 µg/mL). The 3-chloro analog **7c** with MIC value of 0.5 µg/mL was the most potent compound. The MIC values of compounds against *A. fumigatus* and *E. dermatitidis* revealed that all compounds exhibited marginal activity. It should be noted that standard drug fluconazole was inactive against filamentous fungi.

By comparing the MIC values of title compounds **7a–f** and their parent oxime **4**, it could be concluded that the phenoxyethyl ether scaffold is essential for antifungal activity. Although halogen

Table 1

The minimum inhibitory concentrations (MICs, $\mu\text{g/mL}$) of test compounds against different fungi.



Compound	R	<i>C. albicans</i>	<i>C. gattii</i>	<i>A. fumigatus</i>	<i>E. dermatitidis</i>
4	—	>64	>64	>64	>128
7a	H	>64	2	32	128
7b	4-Cl	>64	4	64	64
7c	3-Cl	>64	0.5	32	64
7d	4-F	>64	4	64	128
7e	3-F	>64	2	64	64
7f	2,4-Cl ₂	>64	2	64	128
Fluconazole		2	>64	>64	>64
Itraconazole		0.25	0.5	4	0.5

substitution had positive effect in some cases depends on its position, but could not significantly improve antifungal activity. However, 3-chloro analog **7c** was 4–8 folds more potent than other halo-substituted congeners against *C. gattii*.

As mentioned above, amphotericin B and fluconazole are the most widely used drugs to treat cryptococcosis. There are few reports concerning the in vitro antifungal susceptibility of *C. gattii*. Assessment of antifungal susceptibility for fluconazole and amphotericin B by Silva et al. have been demonstrated that the fluconazole had MICs ranged from 1 to 64 $\mu\text{g/mL}$, while the MICs for amphotericin B were low, ranging from 0.12 to 0.5 $\mu\text{g/mL}$ [15].

In our study, since the designed compounds were structurally related to azole antifungals, thus we tested them side-by-side to the standard azole drugs, fluconazole and itraconazole. The susceptibility testing of designed compounds against different fungi strains revealed that *C. gattii* is more susceptible. Particularly, our data showed that all new compounds tested possess low MIC values against *C. gattii*. The results of our antifungal activity studies, together with the selectivity displayed by our compounds against *C. gattii*, introduces new lead compounds in the development of novel antifungal drugs for treatment of cryptococcal infections. Cryptococcal infections and specially infections caused by *C. gattii* are life-threatening complications for immunocompromised hosts, producing fatal cryptococcosis in patients who have undergone organ transplants and being the main cause of fatal meningoencephalitis in AIDS patients. Thus the designed compounds acting against this fungal pathogen are highly desirable for further in vivo and clinical studies.

4.2. Docking studies

We also accomplished a preliminary study in order to predict how the newly synthesized compounds might interact with the target enzyme lanosterol 14 α -demethylase of cryptococci through computer molecular modeling. It is well known that in the absence of crystal structure of related enzyme, homology modeling is a valuable tool for gaining insight into the interaction between inhibitor and P450-dependent enzymes [16,17].

Herein, we constructed the model of cryptococcal lanosterol 14 α -demethylase by homology modeling on the basis of the reported crystal structure of cytochrome P450 14 α -sterol demethylase of

Mycobacterium tuberculosis (MtCYP51). The crystal structure of MtCYP51 complexed with 4-phenylimidazole (PDB code 1E9X) was retrieved from the Brookhaven Protein Data Bank (www.rcsb.org) and used as a template for homology modeling of *C. neoformans* serotype A CYP51-14 α -demethylase (CnCYP51, SWISS-Prot accession number Q870D1).

As shown in Fig. 2, the sequence of CnCYP51 with that of MtCYP51 was aligned using SWISS-MODEL [18]. The first 57 residues at the N-terminus of CnCYP51 were deleted since, MtCYP51 lacks the N-terminal transmembrane domain found in fungal CYP51 proteins and the 57 N-terminal residues of CnCYP51 were assumed to constitute the membrane binding region and had no counterpart in the catalytic domain.

The obtained 3D model of CnCYP51 built by SWISS-MODEL was subjected to energy minimization using Gaussian98 with Amber96 force field in order to get a stable low energy conformation. After energy minimization, 100 ps molecular dynamic simulations were performed at constant temperature (298 K) and pressure ($P = 1$ atm) using an integration time step of 2 fs with Amber96 force field in an implicit solvent model. OpenMM 5.0 (Simbios, an NIH National Center for Physics Based Simulation of Biological Structures) was used for molecular dynamic (MD) simulations [19]. The root mean square deviation (RMSD) of heavy atoms of protein as a function of time was recorded during simulation which shows the relative structural drift or stability of the structure (Supplementary material). The potential energy of the CnCYP51 model decreased substantially and was stabilized after 100 ps dynamic simulations. The structure of the CnCYP51 model deviated rapidly from the initial structure within the first 60 ps of the MD simulation. This increase in the RMSD is due to the optimization of the interactions within the protein structure. After about 100 ps, the total RMSD of the CnCYP51 model was stabilized at around 1.9 Å, suggesting that this simulation time is sufficient for stabilizing a fully relaxed model.

Ramachandran plot was obtained to assess the stereochemical quality and the geometrical accuracy of the modeled protein (Fig. 3). Ramachandran plot is an interesting parameter for the assessment of protein quality by the means of ϕ/ψ -angle distribution of the protein structure after dynamic simulation. For the CnCYP51 model, 90.5% of the residues were in the favored regions, 6.6% in the allowed regions and 2.9% in disallowed regions. Thus, a total of 97.1% of the residues of the modeled CnCYP51 structure after MD simulation were in the two core (favored and allowed) regions. These data indicated that the backbone dihedral angles ϕ and ψ in the model were reasonable. The residues in disallowed regions are found far away from the active site (Fig. 3).

In order to clarify the binding mode of the newly synthesized azoles in the active site of CnCYP51 and to provide more straightforward information into the interactions between ligand and enzyme for further rational drug design, molecular docking was performed using AutoDock 4.2 [20]. Energy minimization and geometry optimization was done on the ligand structures prior to any docking calculation. Itraconazole as a reference drug was docked into the active site of modeled CnCYP51 (Supplementary material). As shown, triazole ring is pointed towards the heme plane and a ring nitrogen atom coordinating the iron ion. The coordinated triazole nitrogen atom is 3.1 Å distant from the heme iron. 2,4-Dichlorophenyl group of itraconazole makes van der Waals and hydrophobic interactions with Tyr74, Met259, Phe82 and Thr78. The successive phenyl-piperazine-phenyl rings are located in a lipophilic part of active site constituted mainly by hydrophobic side chains of Tyr333, Phe183 and His263. Triazolone ring is situated in a polar region and hydrogen bonded to the polar side chains of Glu177, Asp180 and Glu262. The ending isobutyl chain makes non-polar interactions with Leu144, Val473 and Ser266. Since itraconazole

TARGET 1e9xA	1	DLPP VVFHYIPWFG SAAYYGEDPY KFLFECRDYK GDLFTFILMG
	1	msav--alpr vsq-ghdehg hleefrtdpi glmqrvrdec gdvgtfqlag
TARGET 1e9xA		ss shhhhh h hhhhhhhhhh ssssssss
		ss shhhhh h hhhhhhhhhh ssssssss
TARGET 1e9xA	45	RRVTVALGPK GNNLSLGGKI SQVSAEEAYT HLTPVFGKG VVYDCPNEML
	48	kqvllsgsh anefffragd ddldqakay- pfmtpifgeg vvf--daspe
TARGET 1e9xA		sssssss hh hhhhhhh sss hhhh hh
		sssssss hh hhhhhhh sss hhhhhh hh
TARGET 1e9xA	95	MQQKKFIKSG LTTESLQSYF PMITSECEDF FTKEVGISPQ KPSATLDLLK
	95	rrkemlhnaa lrgeqmkgaha atiedqvrmm iadwg----- -eageidlld
TARGET 1e9xA		hhhhh hh hhhhhhh hhhhhhhhhh h sss ssshh
		hhhhh hh hhhhhhh hhhhhhhhhh h ssssssshh
TARGET 1e9xA	145	SMSELIILTA SRTLQKQEVRL ESLNGQFAKY YEDLDGGFTP LNFMPNPLPL
	139	ffaeltiyts sacligkkfr dqldgrfakl yhelergtdp layvdpylpi
TARGET 1e9xA		hhhhhhhhhhh hhhh hhh h hhhh hhhhhh h
		hhhhhhhhhhh hhhh hhh h hhhh hhhhhh hhhh
TARGET 1e9xA	195	PSYKRRDEAQ KAMSDFYLKI MENRRKGESD --HEHDMIEN LQSCYRN-G
	189	esfrrrdear nglvalvadi mngrianppt dksdrdmldv liaavkaetgt
TARGET 1e9xA		hhhhhhhhhhh hhhhhhhhhh hhhhhh hhhh hhh
		hhhhhhhhhhh hhhhhhhhhh hhhhhh hhhh hhh
TARGET 1e9xA	242	VPLSDRDIAH IMIALLMAGQ HTSSATSSWT LLHLADRPDV VEALYQEQQQ
	239	prfsadeitg mfishmmfagh htssgtaswt lielmrhrda yaavidelde
TARGET 1e9xA		hhhhh hhhh hhh hhhhhhhhhh hhhh hh hhhhhhhhhh
		hhhhh hhhh hhh hhhhhhhhhh hhhh hh hhhhhhhhhh
TARGET 1e9xA	292	KLGNPDGTFR DYKYEDLKEI PIMDSIIRET LRMHAPIHSI YRKVLSDIPV
	289	lygdg----r svsfhalrqi pqlenvlket lrlhplliil mrvakgefe-
TARGET 1e9xA		h hhhh hhhhhhhhhh hhh s ssssssss
		hhhhh hhhhhhhhhh hhh s ssssssss
TARGET 1e9xA	342	PPSLAPSEN GQYIIPKSHY IMAAPGVSQM DPRIWQDAKV WNPARWHDEK
	334	-----v qghrihegdI vaaspaisnr ipedfdpdpd fvparyeqpr
TARGET 1e9xA		sssss sss hhhh hh
		s ssssssss sss hhhh hh
TARGET 1e9xA	392	GFRAAAAMAQY SKAEQVDYGF GSVSKGTESP YQPFAGAGRHR CVGEQFAYTQ
	375	qed----- -llnrwt wipfgagrhr cvgaafaimq
TARGET 1e9xA		sssss sss sss hhhhhh
		hh hh hhhhhh
TARGET 1e9xA	442	LSTIFTYVVR NFTLKLAVP- KFPETNYRTM IVQPNNP-LV TFTLRN
	404	ikaifsvllr eyefemaqpp esyrndhskm vvqlaqpacv ryrrrt-

Fig. 2. Alignment of the amino acid sequences of cytochrome P450 14- α -sterol demethylase of *Cryptococcus neoformans* and *Mycobacterium tuberculosis*.

has a very long side chain, the terminal isobutyl group reached the entrance of substrate accessing channel to the active site.

As discussed above, compound **7c** bearing (3-chlorophenoxy) ethyl moiety attached to the (*E*)-oxime, was the most potent

compound against *C. gattii*. Thus, this compound was considered for further molecular and computational analysis. Figs. 4 and 5 show the binding mode of the two enantiomeric forms (*R* and *S*) of compound **7c** in the CnCYP51 active site. The chroman

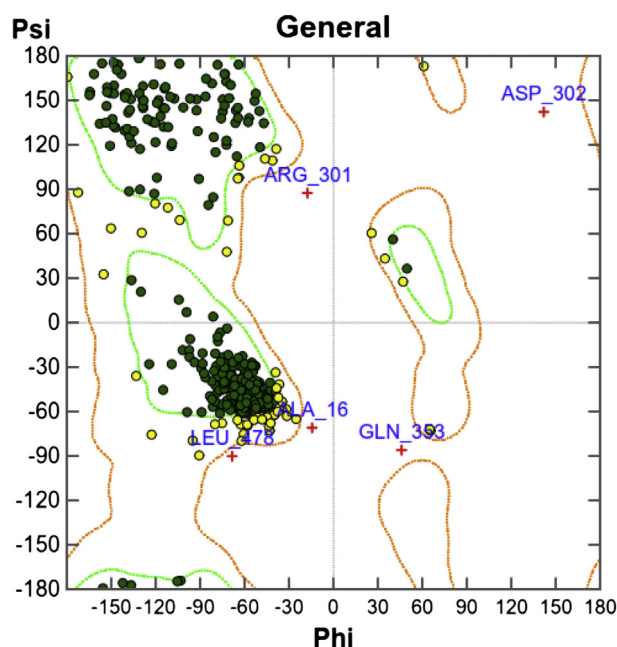


Fig. 3. Ramachandran plot for the last frame of the molecular dynamic simulation of the modeled CnCYP51. Amino acids in the favored regions are in green, in the allowed regions in yellow and in the disallowed regions are represented in red signs. (For interpretation of the references to color in this figure legend, the reader is referred to the web version of this article.)

framework and the imidazole ring of one enantiomer are superposed on those of the other enantiomer and occupy exactly the same regions in the active site with surrounding amino acids Tyr74, Tyr333, Ala73 and Thr75. However, 3-chlorophenyl group is oriented differently in the (*R*) and (*S*)-enantiomers. In the (*R*)-enantiomer of **7c**, it resides as 2,4-dichlorophenyl part of itraconazole with the same interacting amino acids. The 3-chlorophenyl side chain of (*S*)-enantiomer has directed towards Tyr20 and Ser331. The imine nitrogen atom in both enantiomers is protonated in physiological environment and hydrogen bonded to the imidazole ring of His263 (3.7 Å). The N-3 nitrogen atom of imidazole in both enantiomers is coordinated to the heme iron with appropriate distance (3.1 Å for (*S*)-enantiomer and 2.8 Å for (*R*)-enantiomer, respectively).

To rationalize the experimental MIC values and to explain the significant potency differences between the inactive compound **4** and target compound **7c** and also itraconazole as a potent drug against *C. neoformans*, the intermolecular energies including van der Waals, hydrogen bonds, desolvation and electrostatic energies as well as estimated free energy of binding (ΔG , kcal/mol) and estimated inhibition constant (K_i , μM) were calculated and are summarized in Table 2. As shown, enantiomeric forms of **7c** have lower intermolecular energy, free energy of binding and inhibition constant of fungal lanosterol 14 α -demethylase than inactive compound **4**. There is not a great difference between the enantiomeric forms of **7c** in the estimated energy values, although (*S*)-enantiomer shows a bit more potency in inhibiting the fungal enzyme. The lowest binding energy and inhibition constant of itraconazole ($\Delta G = -7.72$ kcal/mol, $K_i = 2.2$ μM) demonstrate its high capability to inhibit lanosterol 14 α -demethylase from *C. neoformans*. Indeed, itraconazole bearing a long side chain forms additional van der Waals contacts and hydrogen bonds with the active site of CnCYP51 (intermolecular energy = -10.24 kcal/mol). As concluded, there is high correlation between the estimated inhibition constants calculated by docking and scoring of compounds in the active site of CnCYP51 and the measured MIC values.

5. Conclusion

In summary, we described a series of imidazolylchromanones containing (phenoxyethyl)-oxime ether moiety as new azole anti-fungals selective against *C. gattii*. All synthesized compounds **7a–f** exhibited potent activity against *C. gattii*. Among them, (3-chlorophenoxy)ethyl analog **7c** with MIC value of 0.5 $\mu g/mL$ was the most potent compound. Our molecular docking studies provided a better insight into the binding of designed compounds within the homology modeled active site of CnCYP51.

6. Experimental

6.1. Chemistry

All starting materials and solvents were purchased from Merck Company and used without further purification. The intermediates 2-phenoxyethyl chloride (**6a**) and 2-(4-chlorophenoxy)ethyl chloride (**6b**) were commercially available materials and purchased from Merck and Sigma–Aldrich companies, respectively. The key intermediate oxime **4** was prepared as previously described method [12]. The progress of the reactions was checked by thin-layer chromatography (TLC) using silica gel 60 F254 plastic sheets (Merck). UV light (254 nm) or iodine vapor were used for visualization. Yields are based on isolated products and were not optimized. Melting points were determined in open glass capillaries using Bibby Stuart Scientific SMP3 apparatus (Stuart Scientific, Stone, UK) and are uncorrected. The IR spectra were recorded on a PerkinElmer FT-IR spectrophotometer. The NMR spectra were obtained using a Bruker 500 spectrometer. In the interpretation of NMR data, chemical shifts are expressed as δ (ppm) with tetramethylsilane (TMS) as internal standard. The multiplicities of signals are reported as follows: s, singlet; d, doublet; t, triplet; q, quartet; br, broad; m, multiplet, and the coupling constants (*J*) are expressed in Hertz (Hz).

6.1.1. General procedure for the synthesis of compounds **6c–f**

A mixture of substituted phenol (10 mmol) and potassium carbonate (15 mmol) in butan-2-one (25 mL) was refluxed for 0.5 h. Then, 1-bromo-2-chloroethane (30 mmol) was added to the reaction mixture and refluxing was continued for 10 h. After completion of the reaction, water (40 mL) was added and the mixture was extracted with diethyl ether several times. The organic phase was washed (10% NaOH solution and water, respectively) and dried (Na_2SO_4). The solvent and the excess of 1-bromo-2-chloroethane were evaporated under reduced pressure to give compounds **6c–f** as oil.

6.1.1.1. 2-(3-Chlorophenoxy)ethyl chloride (6c). Yield 75%; 1H NMR (500 MHz, $CDCl_3$) δ : 3.82 (t, *J* = 5.4 Hz, 2H, CH_2), 4.23 (t, *J* = 5.4 Hz, 2H, CH_2), 6.82 (d, *J* = 7.5 Hz, 1H, H-6), 6.93 (s, 1H, H-2), 6.98 (d, *J* = 7.5 Hz, 1H, H-4), 7.22 (t, *J* = 7.5 Hz, 1H, H-5).

6.1.1.2. 2-(4-Fluorophenoxy)ethyl chloride (6d). Yield 68%; 1H NMR (500 MHz, $CDCl_3$) δ : 3.81 (t, *J* = 5.4 Hz, 2H, CH_2), 4.20 (t, *J* = 5.4 Hz, 2H, CH_2), 6.86–7.03 (m, 4H, phenyl H).

6.1.1.3. 2-(3-Fluorophenoxy)ethyl chloride (6e). Yield 70%; 1H NMR (500 MHz, $CDCl_3$) δ : 3.83 (t, *J* = 5.5 Hz, 2H, CH_2), 4.23 (t, *J* = 5.5 Hz, 2H, CH_2), 6.62–6.74 (m, 3H, H-2, H-4 and H-6), 7.15–7.30 (m, 1H, H-5).

6.1.1.4. 2-(2,4-Dichlorophenoxy)ethyl chloride (6f). Yield 72%; 1H NMR (500 MHz, $CDCl_3$) δ : 3.86 (t, *J* = 5.4 Hz, 2H, CH_2), 4.27 (t, *J* = 5.4 Hz, 2H, CH_2), 6.88 (d, *J* = 8.5 Hz, 1H, H-6), 7.20 (d, *J* = 8.5 Hz, 1H, H-5), 7.40 (s, 1H, H-3).

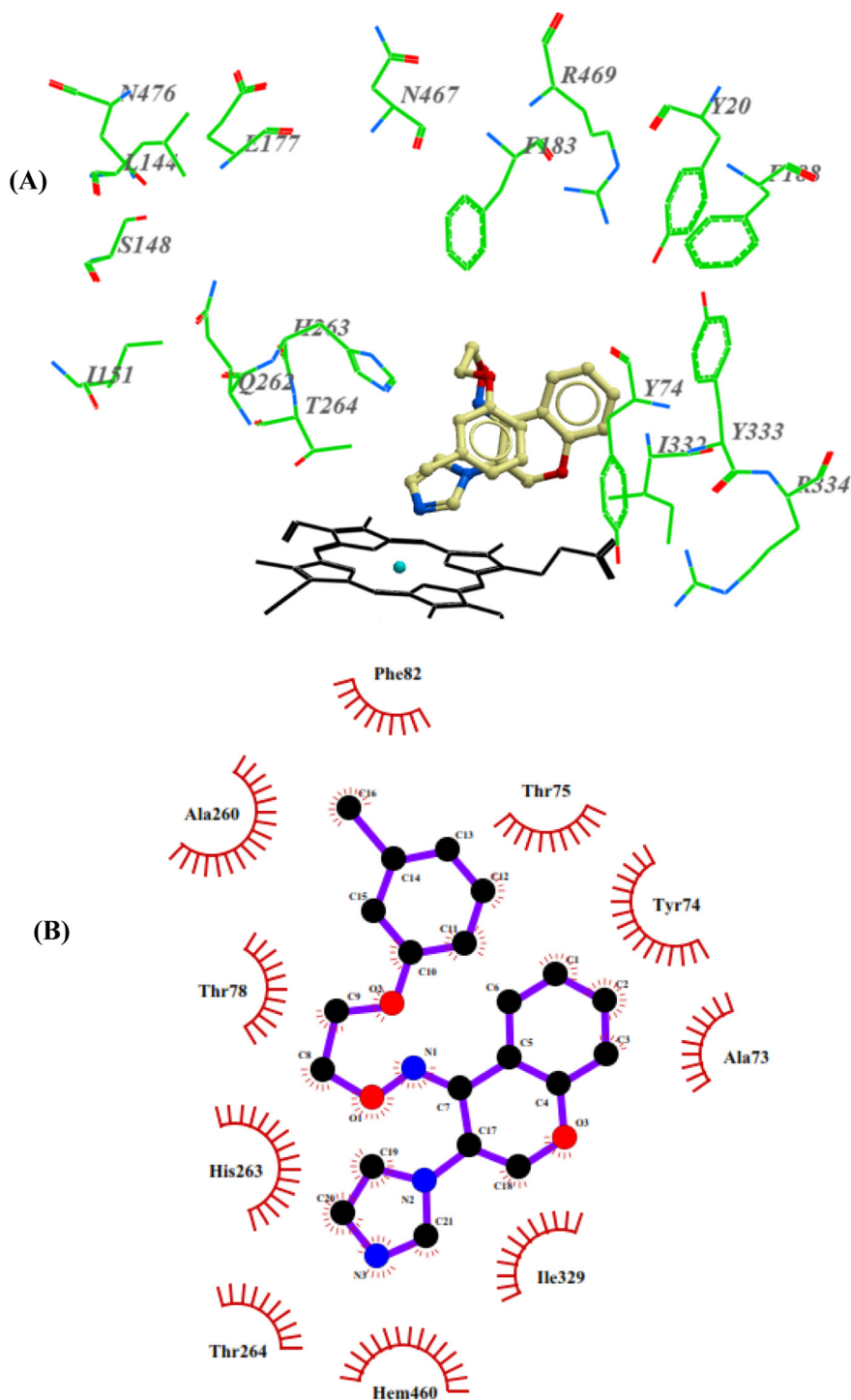


Fig. 4. (A) Binding mode of **R-7c** in the active site of CnCYP51. For clarity only amino acids within 7 Å distant from the docked ligand are shown. (B) 2D map of **R-7c** in the active site of CnCYP51.

6.1.2. General procedure for the synthesis of compounds **7a–f**

A solution of 3-imidazolyl-4-chromanone-(*E*)-oxime (**4**, 0.75 mmol) in dry DMF (1.5 mL) was mixed with a suspension of NaH (18 mg, 0.75 mmol) in dry DMF (1.5 mL). The reaction mixture was stirred at room temperature for 0.5 h. Then, a solution of phenoxyethyl chloride derivative **6** (0.825 mmol) in dry DMF (1 mL) was added gradually and stirring was continued at room temperature for 2 days. After completion of the reaction, the reaction mixture was poured into water (20 mL) and left in refrigerator

overnight. The separated viscous oil was dissolved in propan-2-ol (2 mL) and treated with 65% HNO₃ (0.07 mL) and the mixture was left in a fridge to form nitrate salts. The precipitated crystals were separated and wash with cold propan-2-ol to give pure compound **7**.

6.1.2.1. (±)-(E)-2,3-Dihydro-3-(1H-imidazol-1-yl)-4H-1-benzopyran-4-one O-(2-phenoxy ethyl) oxime nitrate (7a). Yield 75%; mp 113–114 °C; IR (KBr, cm⁻¹) ν_{\max} : 1601 (C=NO). ¹H NMR (500 MHz,

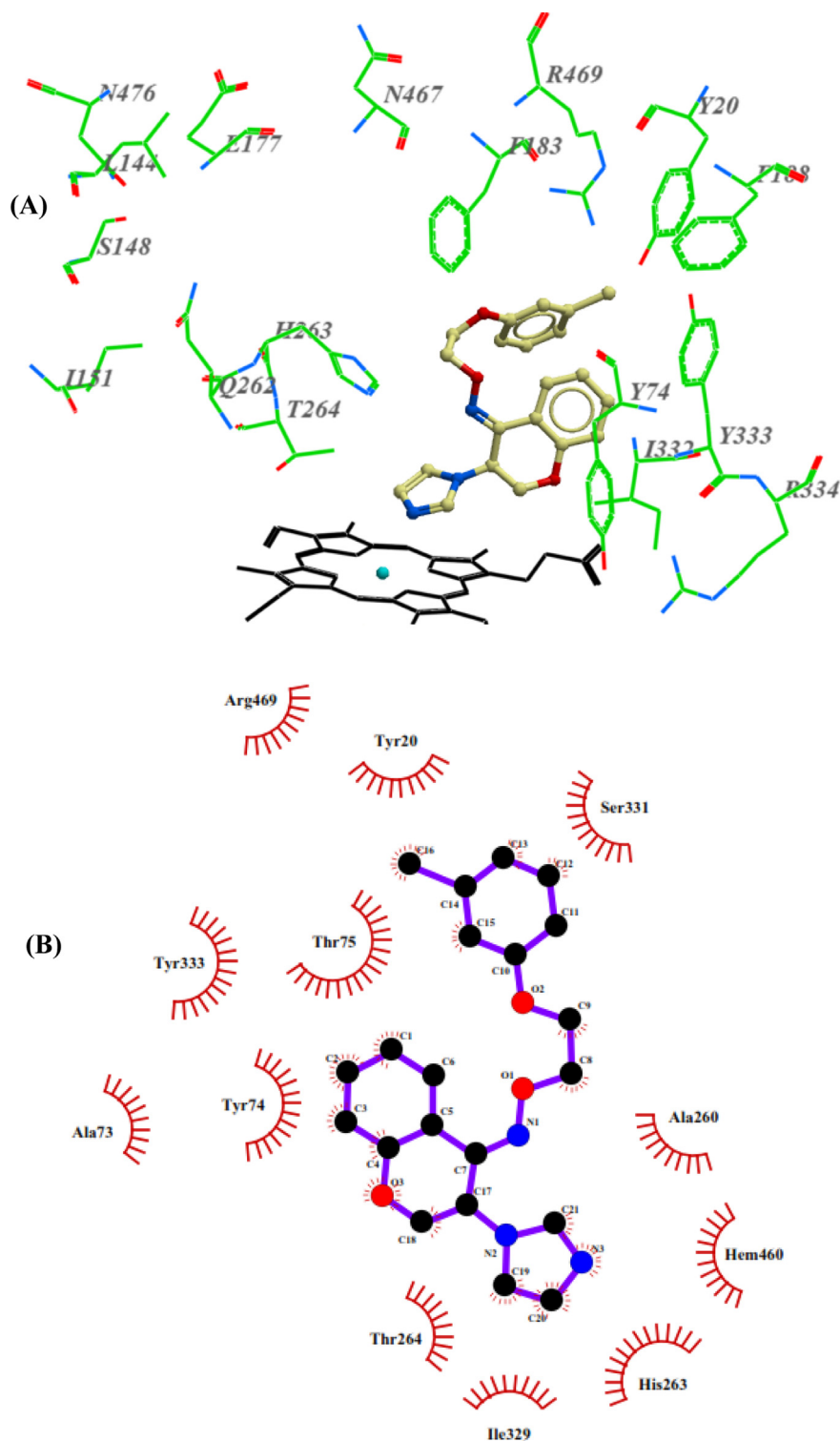


Fig. 5. (A) Binding mode of **S-7c** in the active site of CnCYP51. For clarity only amino acids within 7 Å distant from the docked ligand are shown. (B) 2D map of **S-7c** in the active site of CnCYP51.

DMSO- d_6) δ : 4.32 (t, $J = 4.4$ Hz, 2H, CH_2), 4.54 (t, $J = 4.4$ Hz, 2H, CH_2), 4.70 (dd, $J = 12.0$ and 3.0 Hz, 1H, chroman H-2a), 5.01 (dd, $J = 12.0$ and 3.6 Hz, 1H, chroman H-2b), 5.64 (dd, $J = 3.6$ and 3.0 Hz, 1H, chroman H-3), 6.90–7.18 (m, 5H, phenyl H-2, H-4 and H-6, chroman H-6 and H-8), 7.28 (t, $J = 7.3$ Hz, 2H, phenyl H-3 and H-5), 7.46 (t, $J = 7.5$ Hz, 1H, chroman H-7), 7.68 (s, 1H, imidazole H-4), 7.72 (s, 1H, imidazole H-5), 8.57 (d, $J = 8.0$ Hz, 1H, chroman H-5), 9.22 (br s, 1H,

imidazole H-2), 14.73 (br s, 1H, NH^+). ^{13}C NMR (125 MHz, DMSO- d_6) δ : 55.7 (C-3, chroman), 65.8 (CH_2), 67.1 (CH_2), 74.0 (C-2, chroman), 113.5 (C-4a, chroman), 114.5 (C-2 and C-6, phenyl), 117.6 (C-8, chroman), 120.5 (C-4, phenyl), 120.7 (C-6, chroman), 121.0 (C-5, imidazole), 121.8 (C-4, imidazole), 129.5 (C-3 and C-5, phenyl), 131.4 (C-5, chroman), 133.2 (C-7, chroman), 135.3 (C-2, imidazole), 141.7 (C-8a, chroman), 154.8 (C-1, phenyl), 158.3 (C-4, chroman). MS (m/z ,

Table 2
Estimated energies (ΔG , kcal/mol) and inhibition constant (K_i , μM) calculated by AutoDock.

Compound	Intermolecular energy		Estimated binding energy (ΔG)	Estimated inhibition constant (K_i)
	VdW + H-bond + desolv. energy	Electrostatic energy		
(S)- 7c	−8.27	−0.13	−6.61	14.28
(R)- 7c	−7.85	−0.24	−6.3	24.26
(S)- 4	−5.53	−0.24	−5.17	161.66
(R)- 4	−6.19	−0.03	−5.5	92.24
Itraconazole	−10.24	−0.17	−7.72	2.2

%; 349 (M^+ , 37), 256 (68), 229 (75), 171 (31), 161 (52), 146 (72), 95 (100), 77 (97), 69 (61). Anal. Calcd for $C_{20}H_{20}N_4O_6$: C, 58.25; H, 4.89; N, 13.59. Found: C, 58.02; H, 4.94; N, 13.59.

6.1.2.2. (\pm)-(E)-2,3-Dihydro-3-(1H-imidazol-1-yl)-4H-1-benzopyran-4-one O-[2-(4-chloro phenoxy) ethyl] oxime nitrate (**7b**). Yield 63%; mp 102–103 °C; IR (KBr, cm^{-1}) ν_{max} : 1603 (C=NO). 1H NMR (500 MHz, DMSO- d_6) δ : 4.32 (t, J = 4.3 Hz, 2H, CH_2), 4.53 (t, J = 4.3 Hz, 2H, CH_2), 4.69 (dd, J = 11.0 and 3.0 Hz, 1H, chroman H-2a), 5.00 (dd, J = 11.0 and 3.6 Hz, 1H, chroman H-2b), 5.63 (dd, J = 3.6 and 3.0 Hz, 1H, chroman H-3), 6.95–7.15 (m, 4H, chroman H-6 and H-8, phenyl H-2 and H-6), 7.30 (d, J = 7.6 Hz, 2H, phenyl H-3 and H-5), 7.46 (t, J = 7.5 Hz, 1H, chroman H-7), 7.68 (s, 1H, imidazole H-4), 7.72 (s, 1H, imidazole H-5), 8.53 (d, J = 8.0 Hz, 1H, chroman H-5), 9.20 (s, 1H, imidazole H-2). ^{13}C NMR (125 MHz, DMSO- d_6) δ : 55.7 (C-3, chroman), 66.3 (CH_2), 67.1 (CH_2), 73.9 (C-2, chroman), 113.5 (C-4a, chroman), 116.3 (C-2 and C-6, phenyl), 117.6 (C-8, chroman), 120.5 (C-6, chroman), 120.9 (C-5, imidazole), 121.8 (C-4, imidazole), 124.5 (C-4, phenyl), 129.2 (C-3 and C-5, phenyl), 131.4 (C-5, chroman), 133.2 (C-7, chroman), 135.2 (C-2, imidazole), 141.8 (C-8a, chroman), 154.8 (C-1, phenyl), 157.1 (C-4, chroman). MS (m/z , %): 383 (M^+ , 8), 315 (16), 278 (35), 256 (28), 229 (32), 212 (41), 188 (27), 161 (100), 144 (40), 128 (74), 111 (90), 95 (57), 75 (60), 58 (67). Anal. Calcd for $C_{20}H_{19}ClN_4O_6$: C, 53.76; H, 4.29; N, 12.54. Found: C, 54.07; H, 4.22; N, 12.61.

6.1.2.3. (\pm)-(E)-2,3-Dihydro-3-(1H-imidazol-1-yl)-4H-1-benzopyran-4-one O-[2-(3-chloro phenoxy) ethyl] oxime nitrate (**7c**). Yield 45%; mp 108–109 °C; IR (KBr, cm^{-1}) ν_{max} : 1598 (C=NO). 1H NMR (500 MHz, DMSO- d_6) δ : 4.37 (t, J = 4.4 Hz, 2H, CH_2), 4.54 (t, J = 4.4 Hz, 2H, CH_2), 4.7 (dd, J = 12.5 and 3.0 Hz, 1H, chroman H-2a), 5.01 (dd, J = 12.5 and 3.6 Hz, 1H, chroman H-2b), 5.63 (dd, J = 3.6 and 3.0 Hz, 1H, chroman H-3), 6.96 (dd, J = 8.3 and 1.9 Hz, 1H, chroman H-8), 7.00–7.11 (m, 4H, chroman H-6, phenyl H-2, H-4 and H-6), 7.30 (t, J = 8.2 Hz, 1H, phenyl H-5), 7.46 (dt, J = 8.3 and 1.4 Hz, 1H, chroman H-7), 7.68 (t, J = 1.5 Hz, 1H, imidazole H-4), 7.71 (t, J = 1.5 Hz, 1H, imidazole H-5), 8.54 (dd, J = 8.0 and 1.4 Hz, 1H, chroman H-5), 9.17 (s, 1H, imidazole H-2), 14.50 (br s, 1H, NH^+). ^{13}C NMR (100 MHz, DMSO- d_6) δ : 56.2 (C-3, chroman), 66.9 (CH_2), 67.6 (CH_2), 74.4 (C-2, chroman), 113.9 (C-4a, chroman), 114.3 (C-6, phenyl), 115.0 (C-2, phenyl), 118.1 (C-8, chroman), 121.1 (C-6, chroman), 121.3 (C-5, imidazole), 121.5 (C-4, imidazole), 122.3 (C-4, phenyl), 131.4 (C-5, phenyl), 131.9 (C-5, chroman), 133.8 (C-7, chroman), 134.2 (C-3, phenyl), 135.8 (C-2, imidazole), 142.3 (C-8a, chroman), 155.3 (C-1, phenyl), 159.8 (C-4, chroman). MS (m/z , %): 383 (M^+ , 2), 373 (77), 348 (22), 316 (22), 289 (19), 254 (20), 229 (21), 161 (55), 135 (100), 111 (33), 78 (42), 51 (20). Anal. Calcd for $C_{20}H_{19}ClN_4O_6$: C, 53.76; H, 4.29; N, 12.54. Found: C, 53.70; H, 4.31; N, 12.60.

6.1.2.4. (\pm)-(E)-2,3-Dihydro-3-(1H-imidazol-1-yl)-4H-1-benzopyran-4-one O-[2-(4-fluoro phenoxy) ethyl] oxime nitrate (**7d**). Yield 44%; mp 120–121 °C; IR (KBr, cm^{-1}) ν_{max} : 1604 (C=NO). 1H NMR (500 MHz, DMSO- d_6) δ : 4.31 (t, J = 4.5 Hz, 2H, CH_2), 4.53 (t, J = 4.5 Hz, 2H, CH_2),

4.71 (dd, J = 12.5 and 3.0 Hz, 1H, chroman H-2a), 5.01 (dd, J = 12.5 and 3.6 Hz, 1H, chroman H-2b), 5.64 (dd, J = 3.6 and 3.0 Hz, 1H, chroman H-3), 6.97–7.01 (m, 2H, chroman H-6 and H-8), 7.06–7.15 (m, 4H, phenyl H), 7.47 (dt, J = 8.1 and 1.3 Hz, 1H, chroman H-7), 7.68 (t, J = 1.6 Hz, 1H, imidazole H-4), 7.72 (t, J = 1.6 Hz, 1H, imidazole H-5), 8.55 (dd, J = 8.1 and 1.3 Hz, 1H, chroman H-5), 9.18 (s, 1H, imidazole H-2), 14.50 (br s, 1H, NH^+). ^{13}C NMR (100 MHz, DMSO- d_6) δ : 56.2 (C-3, chroman), 67.1 (CH_2), 67.6 (CH_2), 74.5 (C-2, chroman), 114.0 (C-4a, chroman), 116.3 (d, J_{CF} = 9.7 Hz, C-3 and C-5, phenyl), 116.4 (d, J_{CF} = 5.1 Hz, C-2 and C-6, phenyl), 118.1 (C-8, chroman), 121.1 (C-6, chroman), 121.5 (C-5, imidazole), 122.3 (C-4, imidazole), 131.9 (C-5, chroman), 133.7 (C-7, chroman), 135.8 (C-2, imidazole), 142.3 (C-8a, chroman), 155.1 (d, J_{CF} = 1.5 Hz, C-1, phenyl), 155.3 (C-4, chroman), 157.1 (d, J_{CF} = 234.5 Hz, C-4, phenyl). MS (m/z , %): 367 (M^+ , 4), 296 (82), 269 (12), 229 (10), 161 (24), 123 (100), 111 (16), 95 (61), 69 (12). Anal. Calcd for $C_{20}H_{19}FN_4O_6$: C, 55.81; H, 4.45; N, 13.02. Found: C, 56.08; H, 4.66; N, 12.94.

6.1.2.5. (\pm)-(E)-2,3-Dihydro-3-(1H-imidazol-1-yl)-4H-1-benzopyran-4-one O-[2-(3-fluoro phenoxy) ethyl] oxime nitrate (**7e**). Yield 84%; mp 116–117 °C; IR (KBr, cm^{-1}) ν_{max} : 1597 (C=NO). 1H NMR (500 MHz, DMSO- d_6) δ : 4.35 (t, J = 4.4 Hz, 2H, CH_2), 4.54 (t, J = 4.4 Hz, 2H, CH_2), 4.70 (dd, J = 12.5 and 3.0 Hz, 1H, chroman H-2a), 5.00 (dd, J = 12.5 and 3.6 Hz, 1H, chroman H-2b), 5.63 (dd, J = 3.6 and 3.0 Hz, 1H, chroman H-3), 6.7–6.88 (m, 3H, chroman H-6 and H-8, and phenyl H-2), 7.05–7.11 (m, 2H, phenyl H-6 and H-4), 7.31 (q, J = 7.2 Hz, 1H, phenyl H-5), 7.46 (dt, J = 8.2 and 1.5 Hz, 1H, chroman H-7), 7.68 (t, J = 1.6 Hz, 1H, imidazole H-4), 7.71 (t, J = 1.6 Hz, imidazole H-5), 8.55 (dd, J = 8.1 and 1.5 Hz, 1H, chroman H-5), 9.17 (s, 1H, imidazole H-2), 14.60 (br s, 1H, NH^+). ^{13}C NMR (100 MHz, DMSO- d_6) δ : 56.2 (C-3, chroman), 66.9 (CH_2), 67.6 (CH_2), 74.4 (C-2, chroman), 102.6 (d, J_{CF} = 24.8 Hz, C-2, phenyl), 107.9 (d, J_{CF} = 21.1 Hz, C-4, phenyl), 111.5 (d, J_{CF} = 2.6 Hz, C-6, phenyl), 113.9 (C-4a, chroman), 118.1 (C-8, chroman), 121.1 (C-6, chroman), 121.5 (C-5, imidazole), 122.3 (C-4, imidazole), 131.2 (d, J_{CF} = 10.1 Hz, C-5, phenyl), 131.9 (C-5, chroman), 133.8 (C-7, chroman), 135.8 (C-2, imidazole), 142.3 (C-8a, chroman), 155.3 (C-4, chroman), 160.3 (d, J_{CF} = 11.1 Hz, C-1, phenyl), 163.4 (d, J_{CF} = 241.5 Hz, C-3, phenyl). MS (m/z , %): 367 (M^+ , 14), 366 (15), 337 (18), 256 (14), 224 (80), 197 (40), 180 (61), 152 (40), 126 (41), 95 (100), 69 (33). Anal. Calcd for $C_{20}H_{19}FN_4O_6$: C, 55.81; H, 4.45; N, 13.02. Found: C, 55.83; H, 4.53; N, 13.25.

6.1.2.6. (\pm)-(E)-2,3-Dihydro-3-(1H-imidazol-1-yl)-4H-1-benzopyran-4-one O-[2-(2,4-dichloro phenoxy)ethyl] oxime nitrate (**7f**). Yield 53%; mp 84–85 °C; IR (KBr, cm^{-1}) ν_{max} : 1606 (C=NO). 1H NMR (500 MHz, DMSO- d_6) δ : 4.43 (t, J = 4.2 Hz, 2H, CH_2), 4.56 (t, J = 4.2 Hz, 2H, CH_2), 4.69 (dd, J = 12.5 and 3.0 Hz, 1H, chroman H-2a), 5.00 (dd, J = 12.5 and 3.4 Hz, 1H, chroman H-2b), 5.63 (dd, J = 3.4 and 3.0 Hz, 1H, chroman H-3), 7.00–7.12 (m, 2H, chroman H-6 and H-8), 7.23 (d, J = 8.9 Hz, 1H, phenyl H-6), 7.36 (dd, J = 8.9 and 2.5 Hz, 1H, phenyl H-5), 7.47 (dt, J = 8.5 and 1.3 Hz, 1H, chroman H-7), 7.56 (d, J = 2.5 Hz, 1H, phenyl H-3), 7.68 (s, 1H, imidazole H-4), 7.72 (s, 1H,

imidazole H-5), 8.57 (dd, $J = 8.0$ and 1.3 Hz, 1H, chroman H-5), 9.19 (s, 1H, imidazole H-2), 14.50 (br s, 1H, NH^+). ^{13}C NMR (100 MHz, DMSO-d_6) δ : 56.1 (C-3, chroman), 67.7 (CH_2), 68.1 (CH_2), 74.2 (C-2, chroman), 113.9 (C-4a, chroman), 116.0 (C-6, phenyl), 118.1 (C-8, chroman), 121.2 (C-6, chroman), 121.4 (C-5, imidazole), 122.2 (C-4, imidazole), 123.0 (C-2, phenyl), 125.2 (C-5, phenyl), 128.6 (C-4, phenyl), 129.8 (C-3, phenyl), 131.9 (C-5, chroman), 133.7 (C-7, chroman), 135.8 (C-2, imidazole), 142.5 (C-8a, chroman), 153.3 (C-1, phenyl), 155.3 (C-4, chroman). MS (m/z , %): 418 (M^+ , 43), 382 (100), 256 (11), 212 (11), 188 (10), 161 (10), 146 (12), 94 (17), 67 (17). Anal. Calcd for $\text{C}_{20}\text{H}_{18}\text{Cl}_2\text{N}_4\text{O}_6$: C, 49.91; H, 3.77; N, 11.64. Found: C, 50.08; H, 3.70; N, 11.76.

6.2. Computational studies

All the computational studies were carried out on a 64 Linux workstation with OpenSUSE 12.3 operating system. All the protein structures have been analyzed and handled with Pymol 1.6.0 (The PyMOL Molecular Graphics System, Version 1.6.0.0 Schrödinger, LLC). The structures of compounds have been prepared using MarvinSketch 5.5.0.1 software (Marvin, version 5.5.0.1, Program B; ChemAxon: Budapest, Hungary; www.chemaxon.com/products). The lowest energy conformations were generated with OpenBabel 2.3.2 software, using the MMFF94s force field [21]. All docking studies have been performed with AutoDock 4.2 software, employing AutoDock Tools (ADT) graphical interface in MGLTools 1.5.6. For the protein and ligands, the Gasteiger charges were computed and the non-polar hydrogen atoms were merged with ADT, thus preparing the appropriate PDBQT files for the molecular docking studies [20].

The Lamarckian genetic algorithm (LGA) was used as a search engine. The active site was defined using AutoGrid 4.2. The grid size was set to $22 \times 22 \times 22$ points with a grid spacing of 1.0 \AA centered on the mass of original ligand in the crystal structure complex. A maximum number of energy evaluations were set to 2,500,000. For each of the 10 independent runs, a maximum number of 27,000 LGA operations were generated on a single population of 150 individuals. Operator weights for crossover, mutation, and elitism were set to 0.80, 0.02, and 1, respectively. 2D map of the ligand-active site complex was made by LigPlot 1.4.4 [22].

Acknowledgments

This work was supported by a grant from the Research Council of Mazandaran University of Medical Sciences, Sari, Iran. A part of this work was related to the Pharm.D thesis of Mojtaba Babazadeh-

Qazijahani (Faculty of Pharmacy, Mazandaran University of Medical Sciences).

Appendix A. Supplementary data

Supplementary data related to this article can be found at <http://dx.doi.org/10.1016/j.ejmech.2014.02.019>.

References

- [1] E.J. Byrnes, K.H. Bartlett, J.R. Perfect, J. Heitman, *Microbes and Infection* 13 (2011) 895–907.
- [2] Z. Tlamçani, M. Er-rami, *Journal of Immunological Techniques in Infectious Diseases* 2 (2013) 2.
- [3] J.D. Nosanchuk, *Recent Patents on Anti-Infective Drug Discovery* 1 (2006) 75–84.
- [4] T.J. Walsh, A. Groll, J. Hiemenz, R. Fleming, E. Roilides, E. Anaissie, *Clinical Microbiology and Infection* 10 (2004) 48–66.
- [5] C.A. Boateng, X.Y. Zhu, M.R. Jacob, S.I. Khan, L.A. Walker, S.Y. Ablordepey, *European Journal of Medicinal Chemistry* 46 (2011) 1789–1797.
- [6] J. Kim, Y.-J. Cho, E. Do, J. Choi, G. Hu, B. Cadieux, J. Chun, Y. Lee, J.W. Kronstad, W.H. Jung, *Fungal Genetics and Biology* 49 (2012) 955–966.
- [7] S.E. Sharp, *Clinical Microbiology Newsletter* 31 (2009) 84–86.
- [8] V. Chaturvedi, S. Chaturvedi, *Trends in Microbiology* 19 (2011) 564–571.
- [9] M. Grimaldi, M. De Rosa, S. Di Marino, M. Scrima, B. Posteraro, M. Sanguinetti, G. Fadda, A. Soriente, A.M. D'Ursi, *Bioorganic & Medicinal Chemistry* 18 (2010) 7985–7990.
- [10] Z. Jiang, Y. Wang, W. Wang, S. Wang, B. Xu, G. Fan, G. Dong, Y. Liu, J. Yao, Z. Miao, W. Zhang, C. Sheng, *European Journal of Medicinal Chemistry* 64 (2013) 16–22.
- [11] J.R. Perfect, G.M. Cox, *Drug Resistance Updates* 2 (1999) 259–269.
- [12] S. Emami, M. Falahati, A. Banifatemi, K. Moshiri, A. Shafiee, *Archiv der Pharmazie* 335 (2002) 318–324.
- [13] Clinical and Laboratory Standards Institute, *Reference Method for Broth Dilution Antifungal Susceptibility Testing of Yeasts*, Approved standard M27-A3, third ed., 2008 (Wayne, PA).
- [14] Clinical and Laboratory Standards Institute, *Reference Method for Broth Dilution Antifungal Susceptibility Testing of Filamentous Fungi*, Approved standard M38-A2, second ed., 2008 (Wayne, PA).
- [15] D.C. Silva, M.A. Martins, M. Walderez Szeszs, L.X. Bonfietti, D. Matos, M.S.C. Melhem, *Diagnostic Microbiology and Infectious Disease* 72 (2012) 332–339.
- [16] M.J. de Groot, *Drug Discovery Today* 11 (2006) 601–606.
- [17] J. Yang, Q. Zhang, M. Liao, M. Xiao, W. Xiao, S. Yang, J. Wan, *Pest Management Science* 65 (2009) 260–265.
- [18] K. Arnold, L. Bordoli, J. Kopp, T. Schwede, *Bioinformatics* 22 (2006) 195–201.
- [19] P. Eastman, M.S. Friedrichs, J.D. Chodera, R.J. Radmer, C.M. Bruns, J.P. Ku, K.A. Beauchamp, T.J. Lane, L.P. Wang, D. Shukla, T. Tye, M. Houston, T. Stich, C. Klein, M.R. Shirts, V.S. Pande, *Journal of Chemistry Theory Computation* 9 (2013) 461–469.
- [20] G.M. Morris, R. Huey, W. Lindstrom, M.F. Sanner, R.K. Belew, D.S. Goodsell, A.J. Olson, *Journal of Computational Chemistry* 30 (2009) 2785–2791.
- [21] N.M. O'Boyle, M. Banck, C.A. James, C. Morley, T. Vandermeersch, G.R. Hutchison, *Journal of Chemical Information* 3 (2011) 33.
- [22] A.C. Wallace, R.A. Laskowski, J.M. Thornton, *Protein Engineering* 8 (1996) 127–134.